Journal of the Australian Ceramic Society (2024) 60:1541–1555
https://doi.org/10.1007/s41779-024-01062-2

RESEARCH

Self-propagating high temperature synthesis (SHS) of ZrC-TiC nanocomposites: Comparison of Mg and Al reductant usage and process optimization

Mehmet Bugdayci[1,2] · Serkan Baslayici[2] · Ozan Coban[3] · Faruk Kaya[4]

Received: 18 August 2023 / Revised: 12 June 2024 / Accepted: 1 July 2024 / Published online: 25 July 2024

Abstract
This study investigated the production of ZrC-TiC composite nanopowders by SHS process in TiO_2-ZrO_2-C-Mg/Al systems. Mg and Al charge stoichiometries and composite charge stoichiometries were optimized for SHS processes. The most precise procedural stages were identified for refining the SHS product; acid concentrations were optimized for Mg usage and an innovative chemical method was developed to eliminate and/or decrease the amount of Al_2O_3 by-product, enabling the utilization of Al. Thermochemical simulations were conducted for thermodynamic evaluations (adiabatic temperature and specific heat) and characterizations were performed by XRD and SEM-EDS analysis. The findings indicated that utilizing both reductants allowed for the synthesis of ZrC-TiC-(Al_2O_3) particles that have considerable surface area and commercial purity. The outcomes demonstrated that Magnesium is a more effective reductant, yet Aluminium, also serves as a viable reductant, even though leading to an increase in process steps, but enabling in-situ formation of sinterability and toughness enhancing Al_2O_3. A novel chemical route including pre-acid leaching, NaOH fusion, water leaching, HCl leaching was identified for the synthesis of ZrC-TiC-Al_2O_3 composite powder where the amount of Al_2O_3 could be organized (according to the desired mechanical properties) by optimization.

Keywords Combustion synthesis · Nano composite · Zirconium carbide · Titanium carbide · Aluminium oxide

Introduction

Zirconium Carbide possesses exceptional attributes such as an exceedingly high melting point, resilience to irradiation, impressive hardness, and resistance to wear. Nevertheless, challenges in sintering, coupled with lower fracture toughness and flexural strength, impose constraints on its application [1–5]. TiC has also other several desirable properties such as good thermal conductivity, and chemical stability. The combination of ZrC and TiC in a composite nanoparticle structure offers the potential for enhanced properties, such as improved sintering behavior and increased fracture toughness. The addition of titanium carbide to zirconium carbide can lower the sintering temperature, making it easier to process and manufacture [6–9].

ZrC and TiC can be expressed as one of the hardest materials known, with a hardness of up to 26 GPa and 29 GPa, respectively. This makes them ideal for use in cutting tools and other applications where high wear resistance is required. Melting point of ZrC is 3303 K, and melting point of TiC is 3140 K which makes them as refractory materials. This means that they can withstand high temperatures without melting. Also has a good thermal conductivity of 21 W/m·K, and 40 W/m·K, respectively. This makes them good conductors of heat, which is useful in applications where heat needs to be transferred efficiently. And they are chemically inert, which means that they do not react

✉ Ozan Coban
ozan.coban@gedik.edu.tr

1 Chemical Engineering Department, Yalova University, Yalova 77200, Turkey

2 Construction Technology Department, Istanbul Medipol University, Istanbul 34810, Turkey

3 Gedik Vocational School, Machinery and Metal Technologies Department, Istanbul Gedik University, Istanbul 34913, Turkey

4 Metallurgical and Material Engineering Department, Istanbul Technical University, Istanbul 34000, Turkey

with most chemicals. This makes them desirable choice for applications where corrosion resistance is important. TiC is a good electrical conductor, with a conductivity of 1.47 × 104 S/cm. This makes it a desirable choice for applications where electrical conductivity is important [10–19]. The production of ZrC-TiC composite is important for the combination of these superior properties. The conducted researches have demonstrated that the mechanical properties can be improved significantly in the production of composite structures. It has been reported that the addition of 20% TiC by volume increased the hardness by 25% in conditions where ZrC and TiC were synthesized together. Also, the results showed that with the addition of over 10% TiC, fracture toughness was also increased. It was also stated that it is significant to determine the rate at which spinodal decomposition, which reduces the fracture toughness, does not occur [20].

There are several methods for the production of both materials separately. These can be listed as carbothermic reduction, mechanical alloying, synthesis from elements, sol-gel, mechanochemical synthesis, solvothermal synthesis. However, combustion synthesis is the most prominent method in terms of ease of industrial application, cost, and product quality. Self-propagating high temperature synthesis (SHS), a method within the category of combustion synthesis methods, has been extensively investigated for the fabrication of such materials in recent times, presenting significant advantages [21–23].

The SHS method used in the production of ZrC-TiC composite nanoparticles allows for the direct synthesis of these materials without the need for additional steps or additives. The method involves the rapid combustion of a mixture of reactants (oxides and reductant), which can generate high temperatures and pressures. These conditions facilitate the formation of the desired composite nanoparticles through reactions between the TiC and ZrC powders [24–35]. This is achieved through the SHS method in ZrO_2-TiO_2-Mg-C system. The use of SHS allows for the direct synthesis of ZrC-TiC composite nanoparticles [36–41]. Acid leaching process is applied to remove undesired phases as a result of SHS processes with magnesiothermic reduction [42].

Another reductant that can be used instead of magnesium is aluminum for SHS systems. However, it is exceedingly difficult to remove the alumina formed after SHS. On the other hand, the formed alumina positively affects the mechanical properties of the 3-component composite material system. It has been seen in the literature that alumina has a positive effect on TiC-Al_2O_3 and ZrC-Al_2O_3 composites. In TiC-Al_2O_3 composites, it has been reported that the Al_2O_3 additive improved the flexural strength, fracture toughness and thermal shock resistance of the material [43–45]. The reason for this was explained as secondary phase particles can blunt cracks, form microcracks and prevent cracks from propagating by deflecting them [43]. Similarly, studies have shown that Al_2O_3 additive significantly increased the mechanical properties of ZrC-Al_2O_3 composite [46, 47]. There are studies reporting that Al_2O_3 additive improves mechanical properties for 3-component ceramic composites [48–52]. On the other hand, controlling the amount of alumina in the SHS product, which is performed by aluminothermic reduction, is important in terms of mechanical properties. It is shown in some studies that as the amount of alumina exceeds a certain value, the mechanical properties of the material were deteriorated [53, 54]. Furthermore, while the mechanical alloying method is generally used in the production of alumina-based or alumina-added composites using pre-produced Al_2O_3 [55], in situ synthesis is provided during the process with SHS and compounds containing Al_2O_3 can be produced in a single step.

Typically, the SHS method employs Mg reductant. This study focused on optimizing the charge stoichiometry for ZrO_2-TiO_2-Mg-C systems, determining the maximum ZrO_2 charge stoichiometry required for successful SHS, and also focused on the optimization of Mg reductant stoichiometry. Despite the challenge for reduction of ZrO_2 due to its high oxygen affinity, this research illustrated that the obstacle can be overcome through composite structure production. Aluminum is also considered suitable for SHS systems. A novel chemical route was established to optimize the product obtained through the reduction process involving Al in the ZrO_2– TiO_2– Al– C system, marking the first application of such a method. The novelties of this study are: (i) optimization of the reductant and charge stoichiometry for the ZrC-TiC composite for the SHS method performed with Mg reductant, (ii) the comparison of the use of Al reductant and the use of Mg reductant, and (iii) development of an innovative chemical route for the control of the amount of Al_2O_3 in the ZrC-TiC-Al_2O_3 composite formed with Al reductant.

Experimental study

Composite structured particles of ZrC-TiC and ZrC-TiC-Al_2O_3 were synthesized by the utilization of oxide raw materials of which purity and particle sizes are presented in Table 1. Based on the chemical reactions indicated in Eqs. 1–2, Mg and Al reductants and carbon black were used.

$$ZrO_2 + TiO_2 + 4\ Mg + 2\ C \rightarrow ZrC + TiC + 4\ MgO \quad (1)$$

$$3\ ZrO_2 + 3\ TiO_2 + 8\ Al + 2\ C \rightarrow 3\ ZrC + 3\ TiC + 4\ Al_2O_3 \quad (2)$$

Experimental workflow chart is presented in Fig. 1. A total of 100 g of raw materials were blended using a turbula

Table 1 The raw materials used in the experimental study

Raw Materials	Purity, wt %	Particle Size, μm
ZrO_2	99.5	< 30
TiO_2	99	< 75
Mg	99.7	75–150
Al	99.8	75–150
C	98	< 30

mixer for 20 min and then subjected to a 2-hour drying period before charged inside a crucible made of copper with the thickness of 5 mm and inner radius of 60 mm. Activation was accomplished through the application of a voltage ranging from 20 to 30 V with a duration of 4–5 s through a direct current power supply, aided by a Cr-Ni filament partially submerged in the charge. Due to the initiation of an exothermic reaction at the upper part of the charge, a combustion wave was generated that propagated downward, extending across the reaction environment. This entire process was finalized within a span of 15–20 s. The porous product obtained was subsequently pulverized using an agate mortar.

Charge stoichiometry optimization was performed to determine the minimum TiO_2 or maximum ZrO_2 stoichiometry required for the SHS reaction to occur. The given ZrC charge stoichiometry values were calculated according to the amount by mass that should be formed in the product theoretically. The reductant stoichiometry has also undergone optimization for SHS involving Mg. Parameters were kept constant in SHS using Al. The outlined experimental methodology is provided in Table 2.

Chemical treatment procedures were implemented to eliminate undesirable phases present in the products acquired through SHS processes. In the case of reduction using Mg, the specific process employed is acid leaching. SHS products resulting from aluminothermic reduction were subjected to purification through a sequence involving pre-leaching, caustic fusion, water leaching, and finally HCl leaching. The chemical reactions occurring during the implemented processes are illustrated in Eq. 3 to 7.

Table 2 Experimental design for SHS processes

Reductant type	Reductant stoichiometry	Charge Stoichiometry (for ZrC)	Specimen code
Mg	90%	50	Mg0.9-50
	100%	50	Mg1.0-50
	110%	50	Mg1.1-50
	120%	60 – 50–40– 30 – 20	Mg1.2-X
Al	120%	50	Al1.2-50

$$MgO_{(s)} + 2\ HCl_{(aq)} \rightarrow MgCl_{2\ (aq)} + H_2O_{(l)} \quad (3)$$

HCl leaching was applied to remove MgO, which is the main undesirable phase formed as a result of reduction with Mg. Unreacted ZrO_2 and TiO_2 and $MgTiO_3$ phases, which may have formed in very small amounts, were similarly removed from the product. Acid leaching is not sufficient to remove Al_2O_3, which is the main undesirable phase formed after the reduction with Al. Because Al_2O_3 is a stable phase, and it is difficult to dissolve in acid. For this reason, it was first converted into water-soluble sodium aluminate by caustic fusion method. (Eq. 4). For this, 200% of the stoichiometrically required amount of NaOH and 10 g of SHS product were mixed and ground together and charged to the furnace, allowing the reaction of molten NaOH and Al_2O_3 at 1000 ^{0}C. When the obtained sodium aluminate was leached with water, Aluminum Hydroxide was formed and precipitated as fine particles and filtered together with the ZrC-TiC product. (Eq. 5). Then, purification was carried out by applying HCl leaching. (Eq. 6). However, as the amount of water increases during HCl leaching, $Al(OH)_3$ crystals will form and precipitate again, so the concentrated acid was heated and the water was evaporated, and the process was carried out by keeping the amount of water low and adding gradually during the leaching process at 90 ^{0}C. In addition to Al_2O_3, the same process steps take place to remove unreacted ZrO_2. (Eq. 7). However, the removal of unreacted TiO_2 does not occur in the same way because the sodium titanate (Na_2TiO_3) that will be formed is insoluble in water. For this, before caustic fusion, TiO_2 removal with HCl leaching was applied.

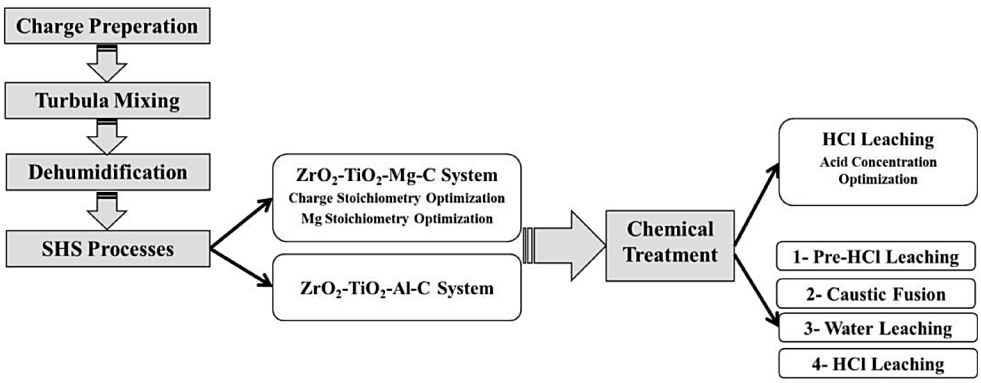

Fig. 1 Flowchart of experimental study

$$Al_2O_{3\,(s)} + 2\,NaOH_{(s)} \rightarrow 2\,NaAlO_{2\,(s)} + H_2O_{(g)} \quad (4)$$

$$NaAlO_{2\,(s)} + 2\,H_2O \rightarrow_{(l)} Al(OH)_{3\,(s)} + NaOH_{(aq)} \quad (5)$$

$$Al(OH)_{3\,(s)} + 3\,HCl_{(aq)} \rightarrow AlCl_{3\,(aq)} + 3\,H_2O_{(l)} \quad (6)$$

$$ZrO_{2\,(s)} + 2\,NaOH_{(s)} \rightarrow Na_2ZrO_{3\,(s)} + H_2O_{(g)} \quad (7)$$

The detailed experimental procedure for the chemical treatment methods is presented in Table 3. The acid concentration was optimized for the refinement of the SHS product obtained by magnesiothermic reduction, and 12 M HCl was used for the SHS products obtained by Aluminothermic reduction.

The acquired products were subjected to characterization through XRD and SEM-EDS analysis. PANalytical Aeris X-Ray powder Diffractometer (with parameters 40 kV– 15 mA) and Zeiss GeminiSEM 500 Field Emission Scanning Electron Microscope equipped with EDS were employed for this analysis.

Table 3 Experimental design for chemical treatment processes

Reductant	Processed Specimen	HCl Concentration (M)	Product
Mg	Mg1.2–50	8	Mg1.0–50 – 8
		10	Mg1.1–50 – 10
		12	Mg1.2–50 – 12
Al	Al1.2–50	12	Al1.2–50 – 12

Thermodynamic background

The adiabatic temperature (T_{ad}) refers to the maximum temperature achievable under adiabatic conditions through the release of heat energy during a reaction. It serves as a crucial parameter in combustion synthesis for obtaining compounds. Merzhanov et al. initially introduced this criterion in 1972, stating that the adiabatic temperature should exceed 1800 K ($T_{ad} > 1800$ K) ($T_{ad} > 1527\ ^0$C) for successful compound formation through combustion synthesis. Over the years, this criterion has been further developed to incorporate melting temperatures of components and kinetic considerations by researchers such as Su et al. in 2014 and Tan et al. in 2021. Evaluating the adiabatic temperature according to Merzhanov et al.'s criterion is the primary requirement in the powder synthesis method utilizing SHS. Another thermodynamic evaluation criterion for the self-propagation mechanism is the specific heat value. It has been revealed that the specific heat value should be 2250–4500 J/g to perform SHS in a controlled manner [56, 57].

The results of the thermochemical simulations performed for the SHS processes, both separately and together, to produce ZrC-TiC composite with SHS are presented in Figs. 2 and 3. Adiabatic temperature changes according to varying mole ratios for Mg and Al reductants are given in Fig. 2. It is also given in Table 4 for 100% stoichiometry values.

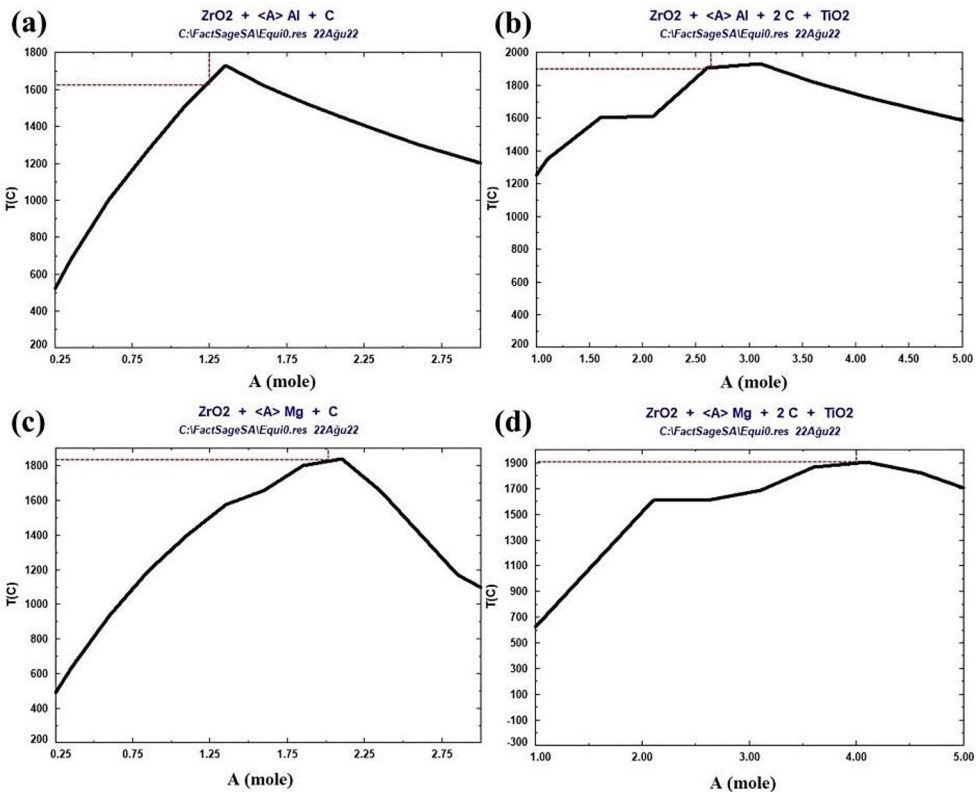

Fig. 2 Thermochemical simulation results for adiabatic temperature change over varying reductant moles (**a**) ZrC synthesis with Al, (**b**) ZrC-TiC synthesis with Al, (**c**) ZrC synthesis with Mg, (**d**) ZrC-TiC synthesis with Mg

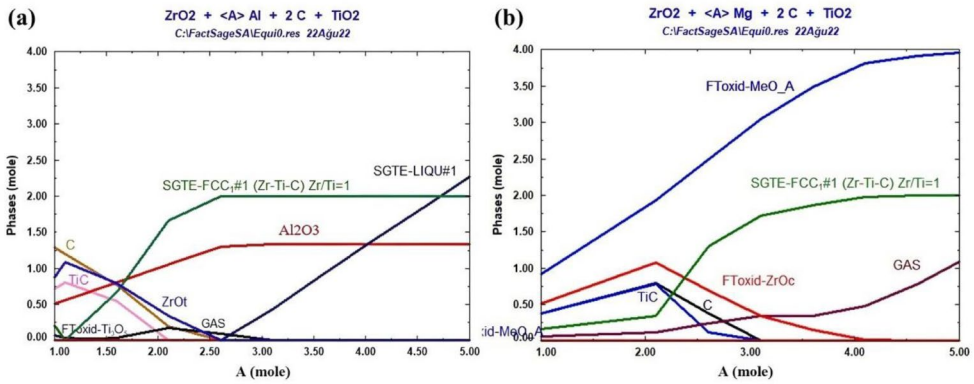

Fig. 3 Thermochemical simulation results for estimated phases change over varying reductant moles (**a**) ZrC-TiC synthesis with Al, (b) ZrC-TiC synthesis with Mg

As can be seen from Fig. 2a; Table 4, while the adiabatic temperature (1630 ^{0}C) is slightly above the critical value at 100% stoichiometry (1.25 moles) in the use of Al reductant for ZrC formation, it is 1900 ^{0}C for the SHS process for ZrC-TiC combined synthesis (Fig. 2b). It is also seen that this increase is low for Mg use (Fig. 2c, d). It has been predicted that the combined SHS application is more important for Al reductant. In addition, for the ZrC-TiC synthesis for the use of Al (Fig. 2b), it is seen that the adiabatic temperature continues to slightly increase up to 120% (3.19 moles) of the Al stoichiometry and begins to decrease above this value. For Mg (Fig. 2d), it is seen that the adiabatic temperature drops to 1800 ^{0}C for a stoichiometry value of 120% (4.8 moles). Therefore, the reductant stoichiometry has been investigated experimentally for the 90–120% range.

Since ZrO_2 is difficult to reduce thermodynamically and the adiabatic temperature is low, it is predicted that the SHS reaction will occur with increasing TiO_2 charge. In Table 4, the calculated specific heat and the adiabatic temperature values determined by thermochemical simulation are given for the reactions for the SHS processes to be conducted using Magnesium and Aluminium reductants. Accordingly, while the specific heat value in the reduction of ZrO_2 with Mg remains below 2250 J/g, it rises above the critical value in the case of SHS with TiO_2. The same is true for reduction with Al. It is predicted that SHS will be realized experimentally by increasing the reductant stoichiometry while approaching the critical value.

Thermochemical simulation results for the phases predicted for the use of Al and Mg reductants for ZrC-TiC synthesis are given in Fig. 3a and b, respectively. With the usage of Al reductant, it is predicted that Al_2O_3 will be formed as well as Zr-Ti-C (Zr/Ti = 1) composite carbides in the structure. In addition, it is expected that the mole ratios of these phases will remain constant above the 2.66 mol value, which is 100% stoichiometry, and Aluminum will remain in the structure. For reduction with Mg, on the other hand, it is predicted that in low reducing stoichiometries, primarily TiO_2 will be reduced to TiC, but ZrO_2 will not be reduced. With the formation of ZrC above about 60% reductant stoichiometry, TiC and free C decreased and Zr-Ti-C (Zr/Ti = 1) composite carbides increased. This increase continues slightly above the 100% stoichiometry value (4 mol). It is seen that the complete reduction of ZrO_2 is completed slightly above 4 moles. For this reason, it is predicted that the yield will increase above 100% stoichiometry.

Results and discussion

Optimization of Composite Charge Stoichiometry

Thermodynamically, the standard free energy of ZrO_2 formation is very low, so its reduction is difficult. In particular, the yield of spontaneous combustion synthesis with metallothermic reduction is low. The SHS process, which enables to benefit from the heat energy released as a result of TiO_2 reduction in the composite structure, is significant. In this sense, optimization of charge stoichiometry calculated on the product to be obtained is important. The XRD results for varying charge stoichiometries are presented in Fig. 4. The findings indicated that the SHS reaction could not take place in the prepared charged state (Mg1.2-60) designed for 60% ZrC. As the reaction enthalpy increased due to the higher TiO_2 ratio, the combustion wave advanced, leading to the successful realization of SHS. In case of Mg charge up to 120% of the theoretical Mg value and charge preparation for obtaining 50%TiC-50%ZrC (Mg1.2-50), a notable quantity of TiC and ZrC were obtained, even though an important amount of unconverted ZrO_2 and some TiO_2 and unreacted Mg remained. The predominant phase observed was MgO, followed by TiC. In the Mg1.2-40 sample, that is, in the case of decreasing ZrO_2 and increasing TiO_2 charge, it was determined that there was a reduction in the Mg content, while the concentration of TiC increased due to the energy generated owing to the increased TiO_2 reduction state. Magnesium Titanate (Mg_2TiO_4) increase was also realized. In the Mg1.2-30 sample, on the other hand, the slight increase

Table 4 Calculated specific heat and adiabatic temperature values for reduction with mg and Al

Mg reductant			Al reductant		
Reaction	Specific heat (J/g)	Adiabatic temperature (^{0}C)	Reaction	Specific heat (J/g)	Adiabatic temperature (^{0}C)
$TiO_2 + 2\,Mg + C \rightarrow TiC + 2\,MgO$	3152,67	2207 [58]	$3TiO_2 + 4\,Al + 3\,C \Diamond 3\,TiC + 2\,Al_2O_3$	2790,35	2273 [59]
$ZrO_2 + 2\,Mg + C \rightarrow ZrC + 2\,MgO$	1739,64	1830	$3ZrO_2 + 4\,Al + 3\,C \Diamond 3\,ZrC + 2\,Al_2O_3$	1364,71	1630
$TiO_2 + ZrO_2 + 4\,Mg + 2C \rightarrow ZrC + TiC + 4\,MgO$	2351,67	1910	$3TiO_2 + 3ZrO_2 + 8\,Al + 6\,C \Diamond 3ZrC + 3TiC + 4\,Al_2O_3$	1974,2	1900

in TiC phase, increase in Mg_2TiO_4 and no increase in ZrC ratio show that SHS efficiency did not increase despite the increasing TiO_2 charge. The same is the case with the Mg1.2-20 sample, and due to the low SHS efficiency and ZrO_2 charge, the amount of ZrC decreased and the amount of TiC remained constant. When the results were evaluated, it was determined that Mg1.2-50 and Mg1.2-40 samples had suitable charge values for the SHS process.

Optimization of Mg stoichiometry

After the charge stoichiometry was optimized, SHS reactions were carried out with a Mg charge of 90 − 120% to determine the optimum Mg stoichiometry. Obtained results are given in Fig. 5. To see the phases obtained as a result of SHS, the results of the Mg1.2-60 sample are also given. It was determined that when the Mg ratio was 90%, the main phase was MgO, a significant amount of unreacted TiO_2 and ZrO_2 phases were present in the structure, and low amounts of carbide phases were formed. In 100% stoichiometry, it was determined that there was a significant increase in the amount of TiC and especially of ZrC. The reduction of the charged oxide phases also shows that the SHS efficiency has increased significantly. At 110% stoichiometry, there was a significant increase in the amount of TiC due to the increased SHS yield, but at the same time the amount of Mg_2TiO_4 has increased. The amount of ZrC also increased significantly. At a stoichiometry of 120%, the reduction of the Mg-titanate (Mg_2TiO_4) phase underscores the significance of maintaining a minimum Mg stoichiometry of 120%. This phase presents challenges in terms of its kinetic removal during the leaching process. Therefore, the Mg1.2-50 sample was determined as optimum. Likewise, Li et al. [8] identified the optimal stoichiometry of magnesium as 120% in the research focused on the SHS production of ZrC within the ZrO_2–Mg–C system.

The XRD analysis outcome of the product derived from the SHS process (TiO_2-ZrO_2-Al-C) conducted with Al as the reductant is presented in Fig. 6, alongside the product obtained using Mg for comparison. While the primary phase comprised Al, notable quantity of TiC and ZrC has also been generated. As anticipated, because of SHS, there was a significant amount of Al_2O_3 formation and some unreacted TiO_2 and ZrO_2 formation. Furthermore, it was established that complex carbide ($ZrAlC_2$) and intermetallic phases (Al_3Ti and Al_3Zr) were also formed. Mehrizi et al. [60] and Wang et al. [17] also reported this formation, which is consistent with our findings. The formations of these phases are given in Eqs. 8–16. The formation of these carbides takes place progressively along with the development of intermediate phases [17, 60–62]. Although temperatures much higher than the temperatures specified in the Equations are

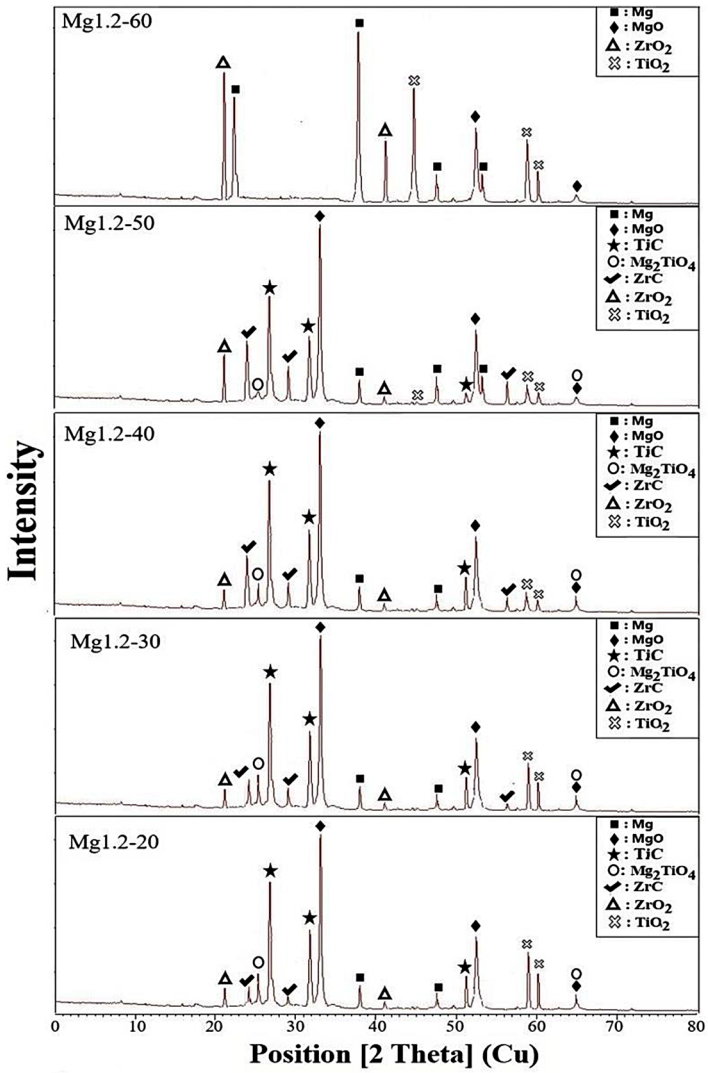

Fig. 4 XRD analysis results of SHS products for varying charge stoichiometry

reached during the SHS process, it is expected that stable intermediate phases are in the SHS product.

$$4Al_{(l)} + 3C_{(s)} = Al_4C_{3(s)} \quad (8)$$

$$Ti + C = TiC \quad (9)$$

$$13Al + 3TiO_2 = 2Al_2O_3 + 3Al_3Ti \quad (10)$$

$$3Al_3Ti + Al_4C_3 = 3TiC + 13Al \left(900^0C \right) \quad (11)$$

$$4Al + 3TiO_2 = 2Al_2O_3 + 3Ti \quad (12)$$

$$13Al + 3ZrO_2 = 3ZrAl_3 + 2Al_2O_3 \quad (13)$$

$$6ZrAl_3 + 5Al_4C_3 = 3Zr_2Al_3C_5 + 29Al \left(900^0C \right) \quad (14)$$

$$Zr_2Al_3C_5 + ZrAl_3 = 2ZrAlC_2 + ZrC + 4Al \quad (15)$$

$$Zr_2Al_3C_5 + 2ZrAl_3 = ZrAlC_2 + 3ZrC + 8Al \left(1150^0C \right) \quad (16)$$

The comparison between reduction with Al and reduction with Mg revealed that the product resulting from reduction with Al contained a higher amount of ZrO_2 and a lesser amount of ZrC and TiC. This observation is consistent with the notion that the adiabatic temperature and specific heat values formed because of the reduction of ZrO_2 with Al are quite low compared to Mg (Table 2).

Chemical Treatment

Following SHS processes involving Magnesium, atmospheric acid leaching processes were conducted using varying concentrations of HCl at a temperature of 90 °C. Obtained XRD analysis results are given in Fig. 7. The sample result of Mg1.2-50, that is SHS product, is also given for comparison. By leaching at 8 M concentration, it was observed that the amount of ZrO_2 decreased slightly,

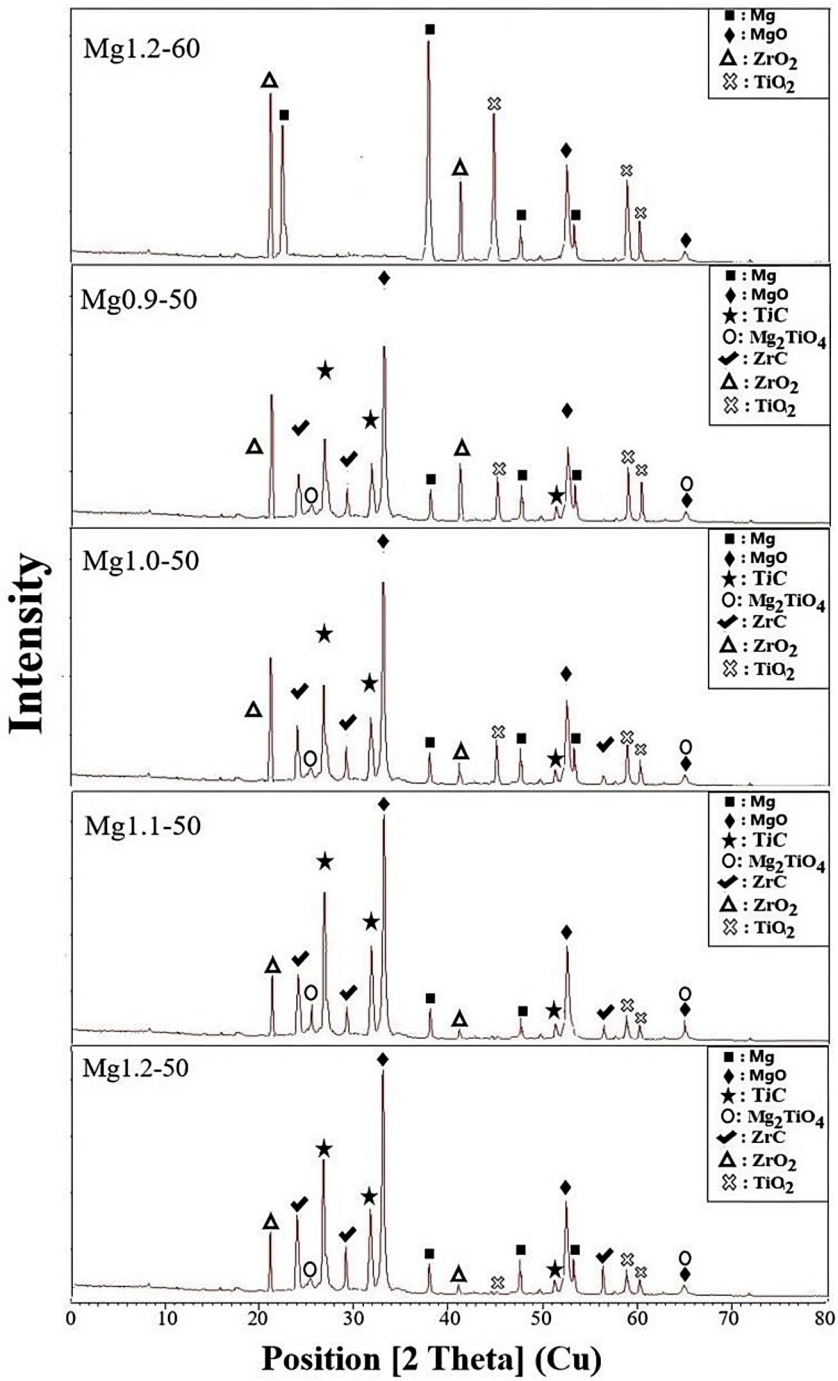

Fig. 5 XRD results of SHS products for varying Mg reductant stoichiometry

MgO could be removed significantly, and the amount of carbide increased slightly. With the increase of the acid concentration to 10 M, it was observed that TiO_2 started to be removed, but the presence of MgO still showed that the concentration was not sufficient. It has been determined that the complete removal of MgO and the beginning of the removal of Mg can only be achieved at 12 M, and that ZrO_2 and TiO_2 can be removed almost completely, and very little amount of Mg_2TiO_4 and Mg remained in the structure. The optimum acid concentration was determined as 12 M. A secondary leaching process was deemed suitable for achieving thorough purification.

The products acquired from SHS involving Aluminium were subjected to the purification steps emphasized before. The XRD analysis of the acquired product, in conjunction with the SHS product, is displayed in Fig. 8. It was ascertained that the predominant constituents of the obtained product were TiC and ZrC. In addition, small quantities of Al_2O_3 and intermetallic phases such as $AlTi_3$ and $AlZr_3$, along with the $ZrAlC_2$ complex carbide, were

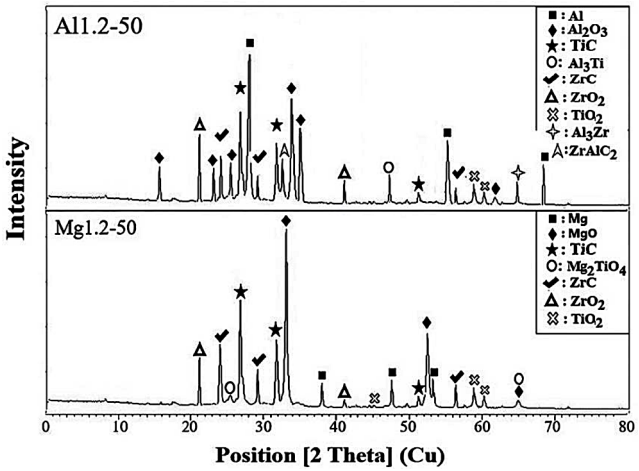

Fig. 6 Comparative XRD results of SHS products for both reductants

detected within the structure. Previous research suggests that the presence of Al_2O_3 in these products could enhance subsequent sintering ability, oxidation resistance, and fracture toughness [63–66]. The intermetallic phases might decrease toughness, however elevate hardness and strength. Residual Aluminum Hydroxide ($Al(OH)_3$) within the structure could potentially transform into Al_2O_3 through heat treatment which should be applied before sintering in order to prevent porosity resulted by H_2O release. Furthermore, it was appraised that any remaining ZrO_2 that couldn't be eliminated might be mitigated by optimizing the NaOH stoichiometry or employing a secondary fusion process.

SEM micrographs of SHS product and chemical treated products for Mg usage are given in Fig. 9. SHS product consists of agglomerates of small TiC-ZrC particles along with coarse MgO particles. After treatment by HCl leaching, MgO could be removed, and product almost completely consisted of ZrC-TiC particles with the size of approx. 300 nm. The particle size was also reduced through chemical treatment. Borovinskaya et al. [67] proposed an approach involving etching SHS powders in a suitable dilute acid or alkaline solution, which dissolves the inclusion-rich layers between crystallites and removes impurities. This method can be termed chemical dispersion. According to Borovinskaya et al., this process causes the sinter cake to break down into crystalline particles of the same size as primary crystallites without altering composition. Therefore, the chemical dispersion process influences not only the chemical and phase composition of the product but also its particle size and surface area. The core of the method lies in the uniform reduction in particle volume due to dissolution in acid or alkali. Alongside particle fragmentation, chemical dispersion facilitates the creation of new channels, pores, and defects, ultimately leading to enhanced specific surface area [68]. This is particularly advantageous for the sintering processes to be applied later.

SEM-EDS results for Mg usage as reductant are given in Fig. 10a, b for SHS product and leach product, respectively. Results revealed that SHS product mainly consisted of course MgO particles. Fine TiC and ZrC particles were also detected on the course MgO surfaces. Chemical treatment (HCl leaching) process removed MgO almost completely. 2% Mg and 8% O content retained within the composition. Secondary leaching could be applied for complete removal. Leached product mainly consisted of TiC and lower amount of ZrC.

SEM micrographs of chemical treated products (Al reduced) are given in Fig. 11. Product consisted of agglomerates of small TiC-ZrC particles along with coarse Al_2O_3 particles. The particle size was a little higher than Mg usage (approx. 400–500 nm). Higher particle size could be caused by caustic fusion process conducted at 1000 ^{0}C. Temperature could be optimized by the considerations of particle size and chemical content. It should also be noted that it may be beneficial to subject these powders obtained before the sintering processes to the ball milling process. Because in this way, Al_2O_3 agglomerates can be broken down, particle size can be reduced and a more homogeneous structure can be obtained. Here, ball mill time optimization according to the sinterability of powders is considered to be another subject to be studied.

SEM-EDS mapping analysis results for Al usage is presented in Fig. 12. Results revealed that product mainly consisted of TiC, ZrC and Al_2O_3. The regions where oxygen was concentrated are also the regions where Al was concentrated, and this shows that the oxides in the structure were largely in the form of Al_2O_3. In regions where carbon was concentrated, mainly Ti, but also Zr concentration was observed. This indicates the presence of TiC and ZrC. While Al and Zr created contrast, that is, they were almost absent in the regions where each other was concentrated, Ti was also located in the regions where Al was concentrated. This suggests the presence of Al_3Ti intermetallic. In general, a heterogenous structure was detected. The potential presence of Al_3Ti, Al_3Zr and $ZrAlC_2$ phases, detected as a result of XRD analysis, was also seen in EDS mapping results. The region where Ti, Al and C concentrations increased (indicated in circles) was seen where Al_3Ti and TiC formation could take place in composite structure.

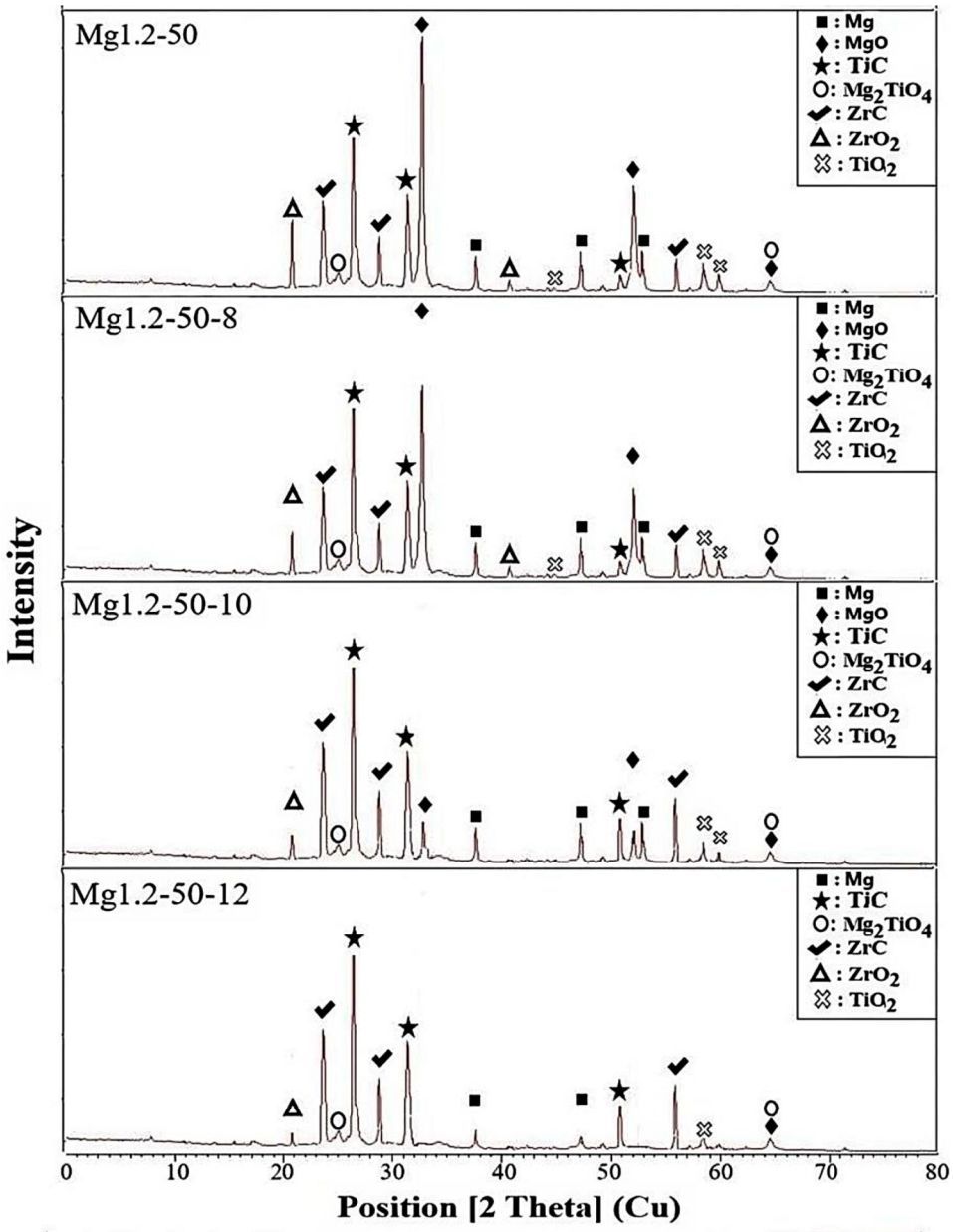

Fig. 7 XRD results of chemical treated products for varying HCl concentration

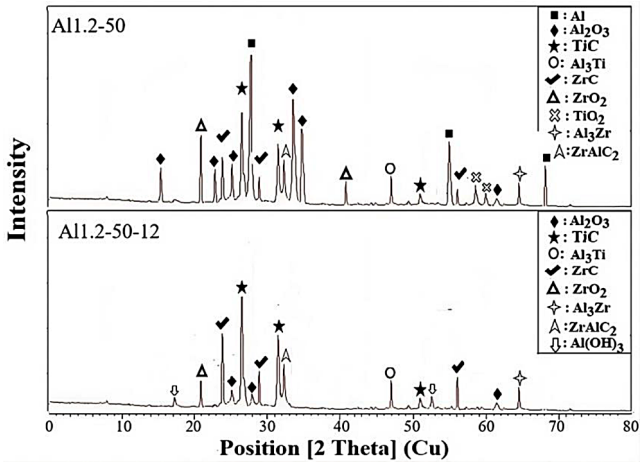

Fig. 8 XRD results of SHS product and chemical treated product for Al usage

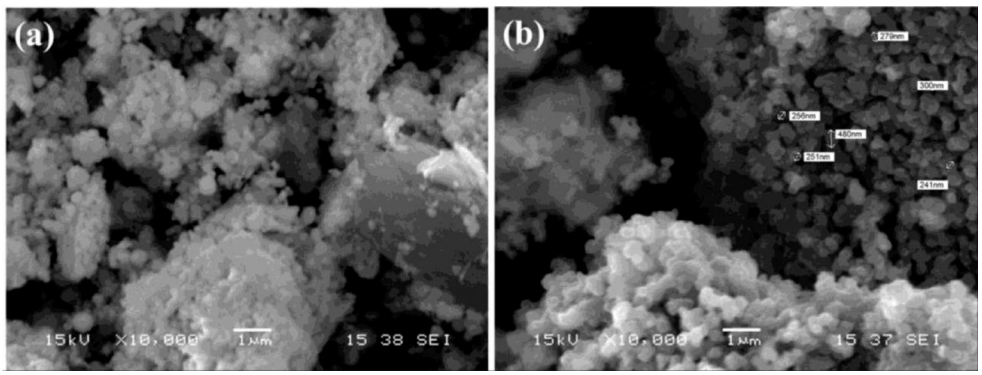

Fig. 9 SEM micrographs for Mg usage as reductant (**a**) SHS product, (**b**) leach product

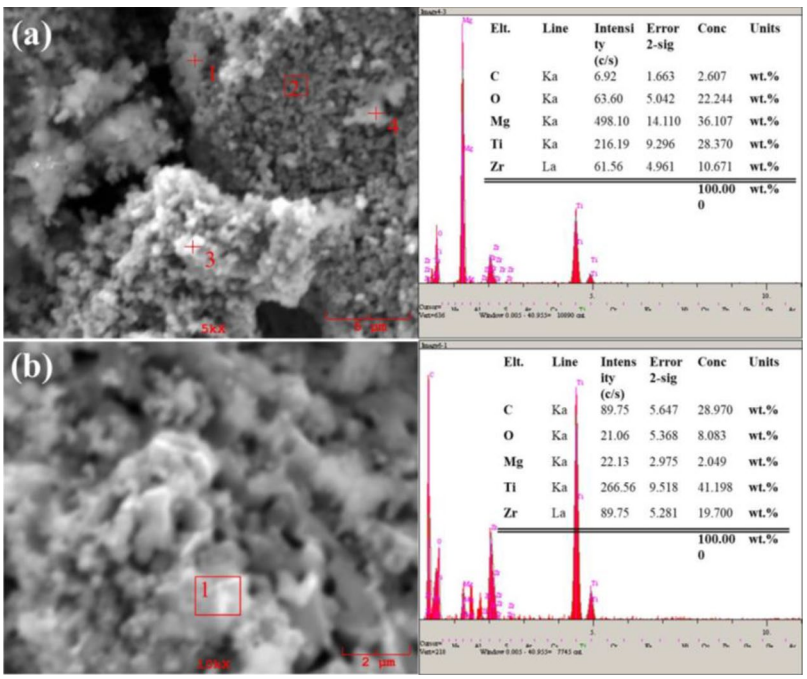

Fig. 10 SEM-EDS results for Mg usage as reductant (**a**) SHS product, (**b**) leach product

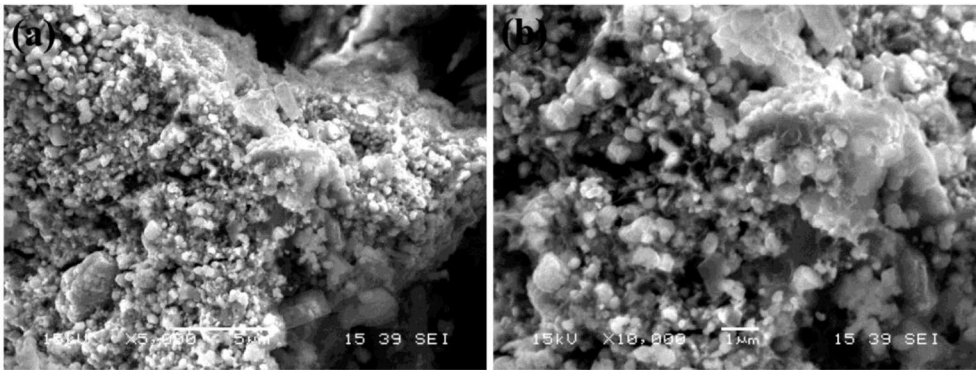

Fig. 11 SEM micrographs of final product for Al usage as reductant (**a**) Mag. 5000X, (**b**) Mag. 10000X

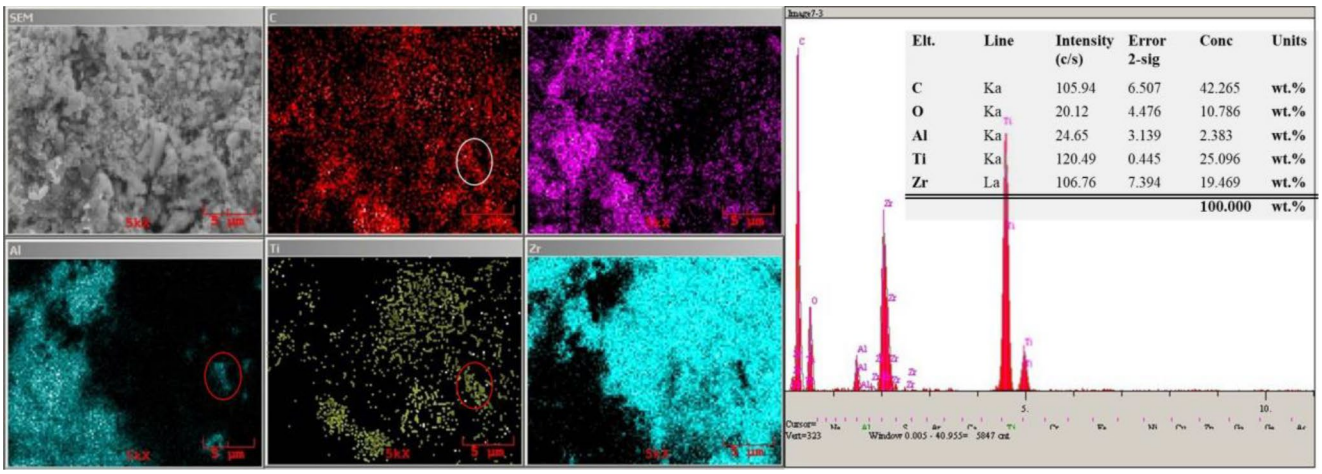

Fig. 12 SEM-EDS results of chemical treated product for Al usage as reductant

Conclusion

The conducted study focused on the fabrication of ZrC-TiC and ZrC-TiC-Al_2O_3 nanocomposite powders using the self-propagating high-temperature synthesis (SHS) method through combustion synthesis. The system employed oxide raw materials in the ZrO_2 - TiO_2 - Mg / Al - C system. Notably, critical phases of the processes utilizing Mg and Al reductants were fine-tuned for optimization. The research demonstrated the feasibility of reducing ZrO_2, which presents challenges due to its oxygen affinity, through the SHS process when integrated into a composite structure.

- Charge stoichiometry was optimized for Mg-containing SHS processes, and it was determined that the maximum ZrO_2 charge for the propagation of the combustion wave should be at the stoichiometry required to obtain 50% ZrC. This value was determined as the optimum value, and it was determined that 40% charge stoichiometry was appropriate to increase the amount of ZrC in the product.
- Mg stoichiometry was optimized, and 110% stoichiometry was found to be appropriate, and 120% stoichiometry was determined as the optimum value, especially in terms of removing Mg-titanate phases. The acid concentration was optimized for purification and 12 M was determined as the optimum value.
- Demonstration of ZrC-TiC synthesis through SHS process utilizing Al reductant has been achieved. It is very difficult to produce only ZrC with SHS using Al reductant, since the specific heat value is below the SHS criterion. It has been shown thermodynamically and experimentally that its synthesis with TiC increases the specific heat value of the reaction and eliminates this difficulty. Complex carbide and intermetallic phases were also identified in the product.
- The products acquired from the SHS process using Al were subjected to an innovative purification method. This led to the synthesis of a ZrC-TiC-Al_2O_3 composite, featuring intermetallic phases and complex carbides that enhance hardness.

As a result of this study, it was suggested that ZrC-TiC composites with superior properties can be produced by using both Mg and Al reductants with the SHS method. It has been shown that the toughness enhancing Al_2O_3 addition can be realized in the process itself by using Al reductant, and this

Al_2O_3 amount can be controlled with the developed innovative chemical route. Academic and industrial information on the synthesis of suitable nanoparticles for the sintering processes to be carried out later has been presented.

Supplementary Information The online version contains supplementary material available at https://doi.org/10.1007/s41779-024-01062-2.

Funding Open access funding provided by the Scientific and Technological Research Council of Türkiye (TÜBİTAK).

Declarations

Conflict of interest On behalf of all authors, the corresponding author states that there is no conflict of interest.

References

1. Landwehr, S.E., Hilmas, G.E., Fahrenholtz, W.G., Talmy, I.G.: Processing of ZrC-Mo cermets for high temperature applications, part II: Pressureless sintering and mechanical properties. J. Am. Ceram. Soc. **91** (2008). https://doi.org/10.1111/j.1551-2916.2007.02231.x
2. Barnier, P., Brodhag, C., Thevenot, F.: Hot-pressing kinetics of zirconium carbide. J. Mater. Sci. **21**, (1986)
3. Umalas, M.: Combined sol-gel and carbothermal synthesis of ZrC-TiC powders for composites. Mater. Chem. Phys. **153** (2015). https://doi.org/10.1016/j.matchemphys.2015.01.017
4. Yung, D.L., Kollo, L., Hussainova, I., Zikin, A.: Reactive sintering of ZrC-TiC composites. in Key Eng. Mater. **527**, (2012). https://doi.org/10.4028/www.scientific.net/kem.527.20
5. Hussainova, I., Voltšihhin, N., Cura, E., Hannula, S.P.: Densification and characterization of spark plasma sintered ZrC-ZrO2 composites. Mater. Sci. Eng., a. **597** (2014). https://doi.org/10.1016/j.msea.2013.12.058
6. Huo, S.: Novel TiC-based composites with enhanced mechanical properties. J. Eur. Ceram. Soc. **41** (2021). https://doi.org/10.1016/j.jeurceramsoc.2021.05.008
7. Liu, L.J.: Microstructures and mechanical properties of TiB2 composite ceramics with co-addition of Ti and TiC fabricated by SPS. Ceram. Int. **49** (2023). https://doi.org/10.1016/j.ceramint.2022.10.230
8. Cheng, L., Xie, Z., Liu, G., Liu, W., Xue, W.: Densification and mechanical properties of TiC by SPS-effects of holding time, sintering temperature and pressure condition. J. Eur. Ceram. Soc. **32** (2012). https://doi.org/10.1016/j.jeurceramsoc.2012.04.017
9. Luo, Y., Li, S., Pan, W., Li, L.: Fabrication and mechanical evaluation of SiC-TiC nanocomposites by SPS. Mater. Lett. **58** (2004). https://doi.org/10.1016/S0167-577X(03)00434-8
10. Osei-Agyemang, E.: Characterizing the ZrC(111)/c-ZrO2(111) hetero-ceramic interface: First principles DFT and Atomistic Thermodynamic modeling. Molecules. **27** (2022). https://doi.org/10.3390/molecules27092954
11. Li, S.: Effects of ZrC content on the microstructure and mechanical property of ZrC/ZTA composites consolidated by hot pressing. J. Alloys Compd. **860** (2021). https://doi.org/10.1016/j.jallcom.2020.158402
12. Xi, L.: ZrC + TiC synergically reinforced metal matrix composites with micro/nanoscale reinforcements prepared by laser powder bed fusion. J. Mater. Res. Technol. **19** (2022). https://doi.org/10.1016/j.jmrt.2022.06.149
13. Prithi, J.A., Shanmugam, R., Sahoo, M.K., Rajalakshmi, N., Rao, G.R.: Evaluation of the durability of ZrC as support material for pt electrocatalysts in PEMFCs: Experimental and computational studies. Int. J. Hydrogen Energy. **47** (2022). https://doi.org/10.1016/j.ijhydene.2022.08.183
14. Zhu, G.: Formation mechanism of spherical TiC in Ni-Ti-C system during combustion synthesis. Materials. **10** (2017). https://doi.org/10.3390/ma10091007
15. Wang, H., Zhu, W., Liu, Y., Zeng, L., Sun, L.: The microwave-assisted green synthesis of TiC powders. Materials. **9** (2016). https://doi.org/10.3390/ma9110904
16. Davoodi, D., Miri, R., Emami, A.H., Tayebi, M., Salahshour, S.: The effect of NiO catalyst on reduction, synthesis and binder content of TiC-Ni nanocomposite. Int. J. Refract. Met. Hard Mater. **88** (2020). https://doi.org/10.1016/j.ijrmhm.2019.105175
17. Wang, Z., Liu, X.: Reaction in the Al-ZrO2-C system. J. Mater. Sci. **40** (2005). https://doi.org/10.1007/s10853-005-0797-2
18. Popov, V.A.: Particulate metal matrix composites development on the basis of in situ synthesis of TiC reinforcing nanoparticles during mechanical alloying. J. Alloys Compd. **707** (2017). https://doi.org/10.1016/j.jallcom.2016.10.051
19. Liu, Z., Rakita, M., Xu, W., Wang, X., Han, Q.: Ultrasound assisted combustion synthesis of TiC in Al-Ti-C system. Ultrason. Sonochem. **27** (2015). https://doi.org/10.1016/j.ultsonch.2015.04.025
20. Acicbe, R.B., Goller, G.: Densification behavior and mechanical properties of spark plasma-sintered ZrC-TiC and ZrC-TiC-CNT composites. J. Mater. Sci. **48** (2013). https://doi.org/10.1007/s10853-012-7024-8
21. Davoodi, D., Hassanzadeh-Tabrizi, S.A., Hossein Emami, A., Salahshour, S.: A low temperature mechanochemical synthesis of nanostructured ZrC powder by a magnesiothermic reaction. Ceram. Int. **41** (2015). https://doi.org/10.1016/j.ceramint.2015.03.034
22. Xu, J., Ma, P., Zou, B., Yang, X.: Reaction behavior and formation mechanism of ZrB2 and ZrC from the Ni-Zr-B4C system during self-propagating high-temperature synthesis. Materials. **16** (2023). https://doi.org/10.3390/ma16010354
23. Najafi, A., Sharifi, F., Mesgari-Abbasi, S., Khalaj, G.: Influence of pH and temperature parameters on the sol-gel synthesis process of meso porous ZrC nanopowder. Ceram. Int. **48** (2022). https://doi.org/10.1016/j.ceramint.2022.05.367
24. Peters, A.B.: Reactive laser synthesis of ultra-high-temperature ceramics HfC, ZrC, TiC, HfN, ZrN, and TiN for additive manufacturing. Ceram. Int. **49** (2023). https://doi.org/10.1016/j.ceramint.2022.11.319
25. Li, J.:: Preparation of ZrC by self-propagating high-temperature synthesis. Kuei Suan Jen Hsueh Pao/Journal Chin. Ceramic Soc. **38**, (2010)
26. Li, J.: Preparation of ZrC by self-propagating high-temperature synthesis. Ceram. Int. **36** (2010). https://doi.org/10.1016/j.ceramint.2010.03.013

27. Li, J.:: Preparation of ZrC powder by self-propagating high-temperature synthesis. in Adv. Mater. Res. **66**, (2009). https://doi.org/10.4028/www.scientific.net/AMR.66.258
28. Ormanci Ozturk, O., Goller, G.: Spark plasma sintering and characterization of ZrC-TiB2 composites. Ceram. Int. **43** (2017). https://doi.org/10.1016/j.ceramint.2017.03.199
29. Munir, Z.A., Lai, W.: The SHS Diagram for TiC. Combust. Sci. Technol. **88**, (1993)
30. Shchukin, A.S., Vadchenko, S.G.: Evolution of gases during SHS of TiC. Int. J. Self Propag. High Temp. Synth. **24** (2015). https://doi.org/10.3103/S1061386215040123
31. Fan, X., Huang, W., Zhou, X., Zou, B.: Preparation and characterization of NiAl–TiC–TiB2 intermetallic matrix composite coatings by atmospheric plasma spraying of SHS powders. Ceram. Int. **46** (2020). https://doi.org/10.1016/j.ceramint.2020.01.052
32. Licheri, R., Orrù, R., Musa, C., Cao, G.: Combination of SHS and SPS techniques for fabrication of fully dense ZrB2-ZrC-SiC composites. Mater. Lett. **62** (2008). https://doi.org/10.1016/j.matlet.2007.05.066
33. Tsuchida, T., Yamamoto, S.: Spark plasma sintering of ZrB2-ZrC powder mixtures synthesized by MA-SHS in air. J. Mater. Sci. **42** (2007). https://doi.org/10.1007/s10853-006-0719-y
34. Tsuchida, T., Yamamoto, S.: Mechanical activation assisted self-propagating high-temperature synthesis of ZrC and ZrB2 in air from Zr/B/C powder mixtures. J. Eur. Ceram. Soc. **24** (2004). https://doi.org/10.1016/S0955-2219(03)00120-1
35. Xu, J.: Fabrication and properties of ZrC-ZrB2/Ni cermet coatings on a magnesium alloy by atmospheric plasma spraying of SHS powders. Ceram. Int. **40** (2014). https://doi.org/10.1016/j.ceramint.2014.07.029
36. Zhang, M., Huo, Y., Huang, M., Fang, Y., Wang, G.: The effect of B4C particle size on the reaction process and product in the Cu-Zr-B 4 C system. J. Asian. Ceam. Soc. **3** (2015). https://doi.org/10.1016/j.jascer.2014.10.006
37. Bartkowski, D., Bartkowska, A., Jurči, P., Przestacki, D.: Influence of Manufacturging Parameters on Microstructure, Chemical Composition, Microhardness, Corrosion and Wear Resistance of ZrC Coatings Produced on Monel® 400 Using Laser Processing Technology. Coatings. **12** (2022). https://doi.org/10.3390/coatings12050651
38. Zhang, M., Huo, Y., Huang, M., Fang, Y., Zou, B.: In situ synthesis and formation mechanism of ZrC and ZrB 2 by combustion synthesis from the Co-Zr-B4C system. J. Asian. Ceam. Soc. **3** (2015). https://doi.org/10.1016/j.jascer.2015.05.005
39. Kerti, I.: Production of TiC reinforced-aluminum composites with the addition of elemental carbon. Mater. Lett. **59** (2005). https://doi.org/10.1016/j.matlet.2005.06.032
40. Wang, J.: Wang Yisan.: In-situ production of Fe-TiC composite. Mater. Lett. **61** (2007). https://doi.org/10.1016/j.matlet.2007.02.011
41. Moreira, A.B., Ribeiro, L.M.M., Vieira, M.F.: Production of TiC-MMCs reinforcements in cast ferrous alloys using in situ methods. *Materials* vol. 14 Preprint at https://doi.org/10.3390/ma14175072 (2021). https://doi.org/10.3390/ma14175072
42. Coban, O., Bugdayci, M., Acma, M.E.: Production of B4C-TiB2 composite powder by self-propagating high-temperature synthesis. J. Aust. Ceram. Soc. **58** (2022). https://doi.org/10.1007/s41779-022-00714-5
43. You, X.Q.: Effect of grain size on thermal shock resistance of Al2O3-TiC ceramics. Ceram. Int. **31** (2005). https://doi.org/10.1016/j.ceramint.2004.02.009
44. Riyadi, T.W.B., Zhang, T., Marchant, D., Zhu, X.: NiAl–TiC–Al2O3 composite formed by self-propagation high-temperature synthesis process: Combustion behaviour, microstructure, and properties. J. Alloys Compd. **805** (2019). https://doi.org/10.1016/j.jallcom.2019.04.349
45. Amel-Farzad, H., Vahdati-Khaki, J., Haerian, A., Youssefi, A.: Combustion wave stability in diluted TiO2/Al/C system in atmospheric air. Solid State Sci. **10** (2008). https://doi.org/10.1016/j.solidstatesciences.2008.03.003
46. Mishra, S.K., Das, S.K., Pathak, L.C.: Sintering behaviour of self-propagating high temperature synthesised ZrB2-Al2O3 composite powder. Mater. Sci. Engineering: A. **426** (2006). https://doi.org/10.1016/j.msea.2006.04.026
47. Sato, K., Ishigaki, T., Kamiya, H., Moriyoshi, Y.: Pressureless sintering behavior of ZrC(O)-Al2O3 composites. Funtai Oyobi Fummatsu Yakin/Journal Japan Soc. Powder Powder Metall. **51** (2004). https://doi.org/10.2497/jjspm.51.741
48. Seidualiyeva, A.J., Kamunur, K., Abdulkarimova, R.G., Yücel, O., Batkal, A.N.: Synthesis of composite materials based on tib2–tic–al2o3 and crb2-al2o3 in the combustion conditions. Eurasian Chem. Technol. J. **23** (2021). https://doi.org/10.18321/ectj1081
49. Gong, F., Zhao, J., Liu, G., Ni, X.: Design and fabrication of TiB2–TiC–Al2O3 gradient composite ceramic tool materials reinforced by VC/Cr3C2 additives. Ceram. Int. **47** (2021). https://doi.org/10.1016/j.ceramint.2021.04.042
50. Cui, H.: Mechanical properties and microstructures of al2o3/tic/tib2 ceramic tool material. Cryst. (Basel). **11** (2021). https://doi.org/10.3390/cryst11060637
51. Zhu, H.G., Chu, D., Wang, H., Min, J., Ai, Y.L.: Study on the reaction mechanism of Al-ZrO2-B4C System. in *Materials Science Forum*. 675–677, (2011). https://doi.org/10.4028/www.scientific.net/MSF.675-677.839
52. Yeh, C.L., Wang, Y.H.: Preparation of ZrB2–SiC–Al2O3 composites by SHS method with aluminothermic reduction. Ceram. Int. **47** (2021). https://doi.org/10.1016/j.ceramint.2020.12.245
53. Latief, F.H., Alsaleh, N.A., Alrasheedi, N., Ataya, S.: Effects of Oxidation and Alumina Addition on the Physical and Mechanical properties of Ti/Al2O3 composites prepared by Semi-powder Metallurgy Method. Oxid. Met. **92** (2019). https://doi.org/10.1007/s11085-019-09923-z
54. Su, W., Zou, J., Sun, L.: Effects of nano-alumina on mechanical properties and wear resistance of WC-8Co cemented carbide by spark plasma sintering. Int. J. Refract. Met. Hard Mater. **92** (2020). https://doi.org/10.1016/j.ijrmhm.2020.105337
55. Yücel, O., Özçelebi, M.A.: Reduction smelting of bursa-uludag tungsten concentrates by the aluminothermic process. Scand. J. Metall. **29** (2000). https://doi.org/10.1034/j.1600-0692.2000.d01-12.x
56. Aydin, H., Elmusa, B.: Fabrication and characterization of Al2O3-TiB2 nanocomposite powder by mechanochemical processing. J. Aust. Ceram. Soc. **57** (2021). https://doi.org/10.1007/s41779-021-00579-0
57. Yücel, O., Cinar, F., Addemir, O., Tekin, A.: The preparation of ferroboron and ferrovanadium by Aluminothermic reduction. High Temp. Mater. Processes (London). **15** (1996). https://doi.org/10.1515/HTMP.1996.15.1-2.103
58. Nersisyan, H.H., Lee, J.H., Won, C.W.: Combustion of TiO2-Mg and TiO2-Mg-C systems in the presence of NaCl to synthesize nanocrystalline Ti and TiC powders. Mater. Res. Bull. **38** (2003). https://doi.org/10.1016/S0025-5408(03)00114-4
59. Lee, J.H., Ko, S.K., Won, C.W.: Combustion characteristics of TiO2/Al/C system. Mater. Res. Bull. **36** (2001). https://doi.org/10.1016/S0025-5408(01)00612-2
60. Mehrizi, M.Z., Beygi, R., Eisaabadi, G.: Synthesis of Al/TiC-Al2O3 nanocomposite by mechanical alloying and subsequent heat treatment. Ceram. Int. **42** (2016). https://doi.org/10.1016/j.ceramint.2016.02.144
61. Hu, Q., Luo, P., Yan, Y.: Microstructures, densification and mechanical properties of TiC-Al2O3-Al composite by field-activated combustion synthesis. Mater. Sci. Engineering: A. **486** (2008). https://doi.org/10.1016/j.msea.2007.08.075

62. Zhao, Y.T., Sun, G.X.: In situ synthesis of novel composites in the system Al-Zr-O. J. Mater. Sci. Lett. **20** (2001). https://doi.org/10.1023/A:1012889221153
63. Xu, J., Zou, B., Tao, S., Zhang, M., Cao, X.: Fabrication and properties of Al2O3–TiB2–TiC/Al metal matrix composite coatings by atmospheric plasma spraying of SHS powders. J. Alloys Compd. **672** (2016). https://doi.org/10.1016/j.jallcom.2016.02.116
64. Li, Z.: Microhardness and wear resistance of Al2O3-TiB2-TiC ceramic coatings on carbon steel fabricated by laser cladding. Ceram. Int. **45** (2019). https://doi.org/10.1016/j.ceramint.2018.09.140
65. Xiao, G.Q., Fu, Y.L., Zhang, Z.W., Hou, A.D.: Mechanism and microstructural evolution of combustion synthesis of ZrB2-Al2O3 composite powders. Ceram. Int. **41** (2015). https://doi.org/10.1016/j.ceramint.2015.01.007
66. Yeh, C.L., Liu, K.T.: Synthesis of TiB2/TiC/Al2O3 and ZrB2/ZrC/Al2O3 composites by low-exotherm Thermitic Combustion with PTFE activation. J. Compos. Sci. **6** (2022). https://doi.org/10.3390/jcs6040111
67. Borovinskaya, I.P., Ignat'eva, T.I., Vershinnikov, V.I., Khurtina, G.G., Sachkova, N.V.: Preparation of Ultra fine boron nitride powders by self-propagating hightemperature synthesis. Inorg. Mater. **39** (2003). https://doi.org/10.1023/A:1024097119257
68. Ignat'eva, T., Borovinskaya, I.: Chemical Dispersion as a method for segregation of Ultrafine and Nanosized powders of SHS Refractory compounds. Eurasian Chem. Technol. J. **15**(2) (2013). https://doi.org/10.18321/ectj148